3D finite-elements kinematic model of the Adria northern region: stress analysis

G. Rossi[1], C. Ebblin[2] and M. Zadro[2]

[1] *Istituto Nazionale di Oceanografia e di Geofisica Sperimentale - OGS, Trieste, Italy*
[2] *Dept. of Earth Sciences, University of Trieste, Italy*

(Received November 9, 2004; accepted December 28, 2004)

ABSTRACT The 3D finite-element method is used in the present work to model the present complex and inhomogeneous stress field on the northern boundary of the so-called Adria microplate (north-eastern Italy). With the aim of providing some possible explanation for the observed stress-strain pattern as a result of plate driving forces, a 3-D linear elastic-static finite-element model of the lithosphere has been constructed, based on geological, seismic and gravimetric evidence. The boundary conditions imposed on the model throughout the experiment depict different scenarios for the kinematics of the region. They are conditions that we try to tune, in order to obtain the best fit with the available observations, i.e. the stress orientations, and the fracturing distribution. In particular, two main kinematic problems are considered: the orientation of the far-field compression acting in the region, and the modalities through which the resulting shortening is achieved. The best fit with the observational data is obtained hypothesizing strike-slip effects at both the eastern and western boundaries. Moreover, as effects of the apparent counterclockwise rotation of the Adria plate, the N-S compression acting at the southern boundary of the model increases with longitude. The results are in agreement with the seismological and deformational observations and with the current hypotheses on the mechanisms that rule continental collision.

1. Introduction

The aim of the present work is to try to reproduce, through a finite-element modelling, the present regional stress field pattern in the northern part of Adria, i.e. north-eastern Italy and its neighbouring regions, Austria, Slovenia, and Croatia (Fig. 1b).

This work was mainly motivated by the results of the analysis of the data of the strain-gauge array, which has been active for more than 20 years in the easternmost part of the study area (Marussi, 1959; Zadro, 1978, Braitenberg, 1999; Rossi *et al.*, 1999). Analyses of the strain-tilt data demonstrated that the strain field in the region is subject to time variations of different frequency and causes, from Earth-tide effects to very long-term variations, involving more than ten-year long periods (Mao *et al.*, 1989, 1990; Rossi and Zadro, 1996; Zadro and Braitenberg, 1999; Braitenberg *et al.*, 2001). In particular, the analysis of the long-term components revealed that the largest amount of strain energy is polarized in two main directions. The first direction is parallel to the dominant regional compression (NNW-SSE), the second one to the compression along the Dinarides (NE-SW), thus suggesting a possible tectonic origin of the phenomenon

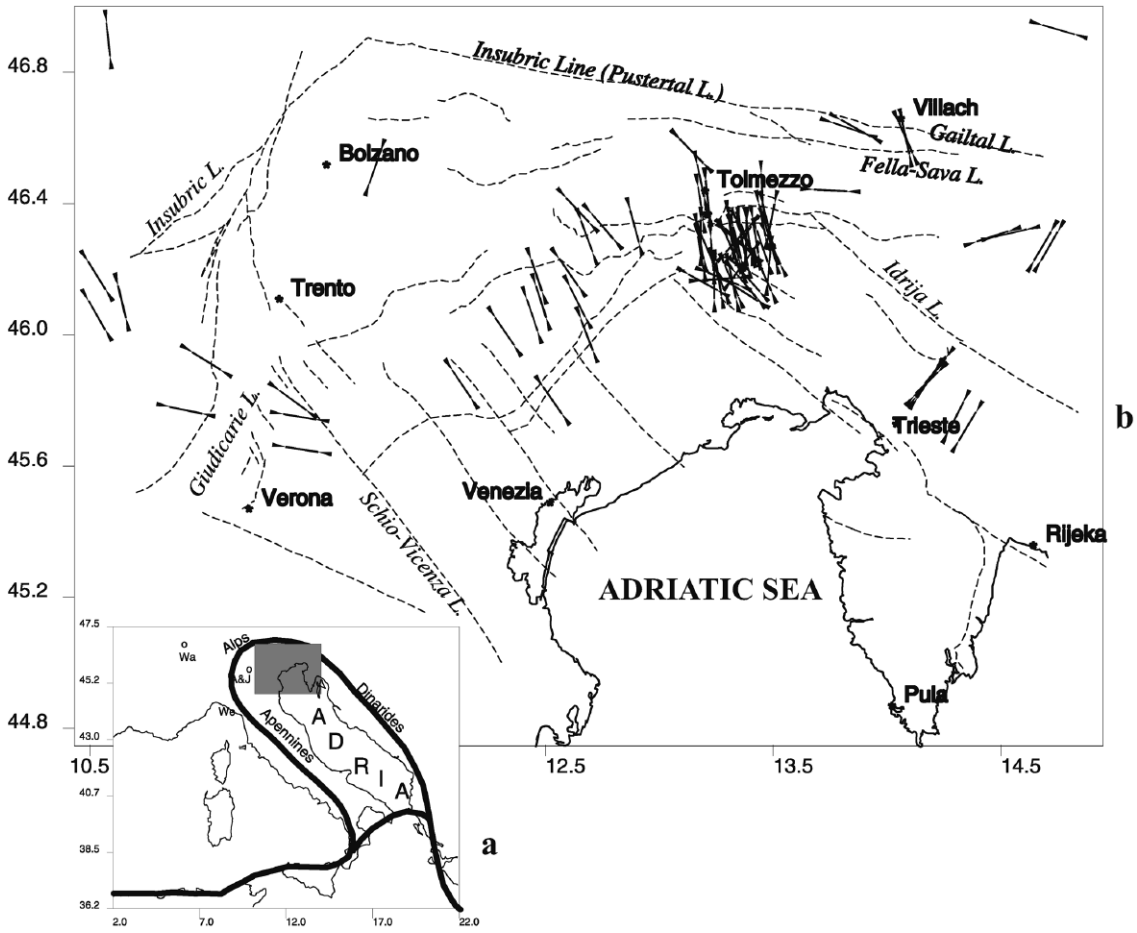

Fig. 1 - a) The area considered in the present work within the Adria frame. The location of the various poles of rotation proposed by Anderson and Jackson (1987; A&J); Westaway (1990; We); Ward (1994; Wa) is shown. b) Schematic map of the region, with the main faults. The arrows show the orientation of the maximum compression inferred from the fault-plane solutions of the main events recorded in the area. The P-axis orientations (see Appendix 1 and Table A1) are from the World Stress Map Project database (Müller *et al.*, 1997) and from Suhadolc (1990).

(Rossi and Zadro, 1996). Hence, the need for a reliable rheologic model of the area covered by the strain gauge array to test and verify the various hypotheses on the observations, while providing some possible explanation in terms of plate driving forces.

In fact, in most recent times the kinematics of the so-called Adria microplate has become one of the most puzzling problems of the Mediterranean area. It is, however, beyond the aims of the present article to enter into the lively debate about Adria-microplate existence, extention and relative motion with respect to Africa and Eurasia (e.g.: Argand, 1924; Horváth, 1984; Anderson and Jackson, 1987; Westaway, 1990; Ward, 1994; Albarello *et al.*, 1995; Altiner, 1999). Our study area is in fact small, when compared with the Adria extension or with the extension of the Mediterranean region, that should be taken into account in an Adria plate modelling. Northern

Adria is, however, a region of great interest, being one of the hinges of the circum-Adriatic active belt. From the fault-plane solutions of the circum-Adriatic major earthquakes, it appears that the extensional deformation acting along the Apennines in a NE-SW direction turns in the Southern Alps to about a N-S compression and finally to a NE-SW oriented compression along the Dinarides (Anderson and Jackson, 1987; Pondrelli *et al.*, 1995). The merging and superposition of the two main structural systems (Alpine and Dinaric) gave here origin to a complex tectonics, dominated by an arch-shaped mountain. Most of the intense seismic activity that affects this region (the most active of the entire Alps area), and that testifies that the collision process with Eurasia started with the Tertiary, is still taking place and is concentrated at the apex of the arch.

In most recent times seismic activity culminated with the Friuli earthquake of May 6, 1976, M=6.4. The fault-plane solutions calculated by different authors agree on the stronger events with a thrust mechanism, with the above mentioned almost uniaxial compression acting in a NNW-SSE /N-S direction (Ebblin, 1976; 1980; Mayer-Rosa *et al.*, 1976; Müller, 1977; Cipar, 1980; Barbano *et al.*, 1984; Slejko *et al.*, 1999; Pondrelli *et al.*, 2001). On a smaller scale, however, deviations from this scheme are observed. To the east, a NE-SW compression is recorded, with a strong shear component (a recent example are the Bovec events, April 12, 1998, M=5.6, and July 12, 2004, M=5.1). The western part of the region shows on the contrary, a NW-SE compression, similar to the rest of the Alps and western Europe, but shear mechanisms are observed around Lake Garda (e.g; Ebblin, 1986; Slejko *et al.*, 1989; Carulli *et al.*, 1990; Suhadolc, 1990; Grünthal and Stromeyer, 1992; Zoback, 1992; Kravanja *et al.*, 1999; Fig. 1b; Table A1). Such directions are confirmed also by the direct in-situ stress-measurements (Grünthal and Stromeyer, 1992) and by the already mentioned strain field observations (Rossi and Zadro, 1996).

In complex areas like this one, when the interpretation of observations may be controversial, numerical modelling of lithospheric deformations provides additional information, by indicating what kind of boundary condition can reproduce the observations (Bassi *et al.*, 1997). Moreover, a 3D numerical modelling enables one to reproduce also the complex 3D geometry of the different lithospheric units and their mutual interaction, and their possible effects on the stress re-orientation.

2. The model

The actual regional stress field in the study area, described by means of forces acting at this plate boundary, is modelled by a finite element code (ABAQUS, HKS Inc). It has already been successfully used for geophysical problems, as in the modelling of periodic, great earthquakes on the San Andreas Fault (Reches *et al.*, 1994). In our analysis, eight-node isoparametric finite-elements (hexahedra or bricks) are used. As known, the reliability of one element decreases as its shape diverges from the parent shape (a cube in 3-D), and hence, in the numerical computation of individual stiffness matrices. To avoid this problem, the ratio of its sizes has been accurately checked, and kept smaller than 3 for each element. Displacements vary linearly along the edges of each element. The stress is constant in each element, being determined at one integration point (the centroid of the element).

The geometry of the principal lithospheric layers of the 3D finite element model is chosen according to the available observations. Some boundary conditions are fixed, whereas the

remaining ones are regarded as conditions that we try to adjust to obtain the best fit with the observations (mainly seismological).

2.1. Geometry

The total dimensions of the model are about 320 km in longitude (10.5° E - 14.5° E), 240 km in latitude (44.8° N - 46.8° N) and about 150 km in depth. The limits of the model have been chosen to avoid boundary effects in the area of interest. Five homogeneous layers constitute the model. From bottom to top: top of the low-velocity channel of the asthenosphere, lid, plus lower,

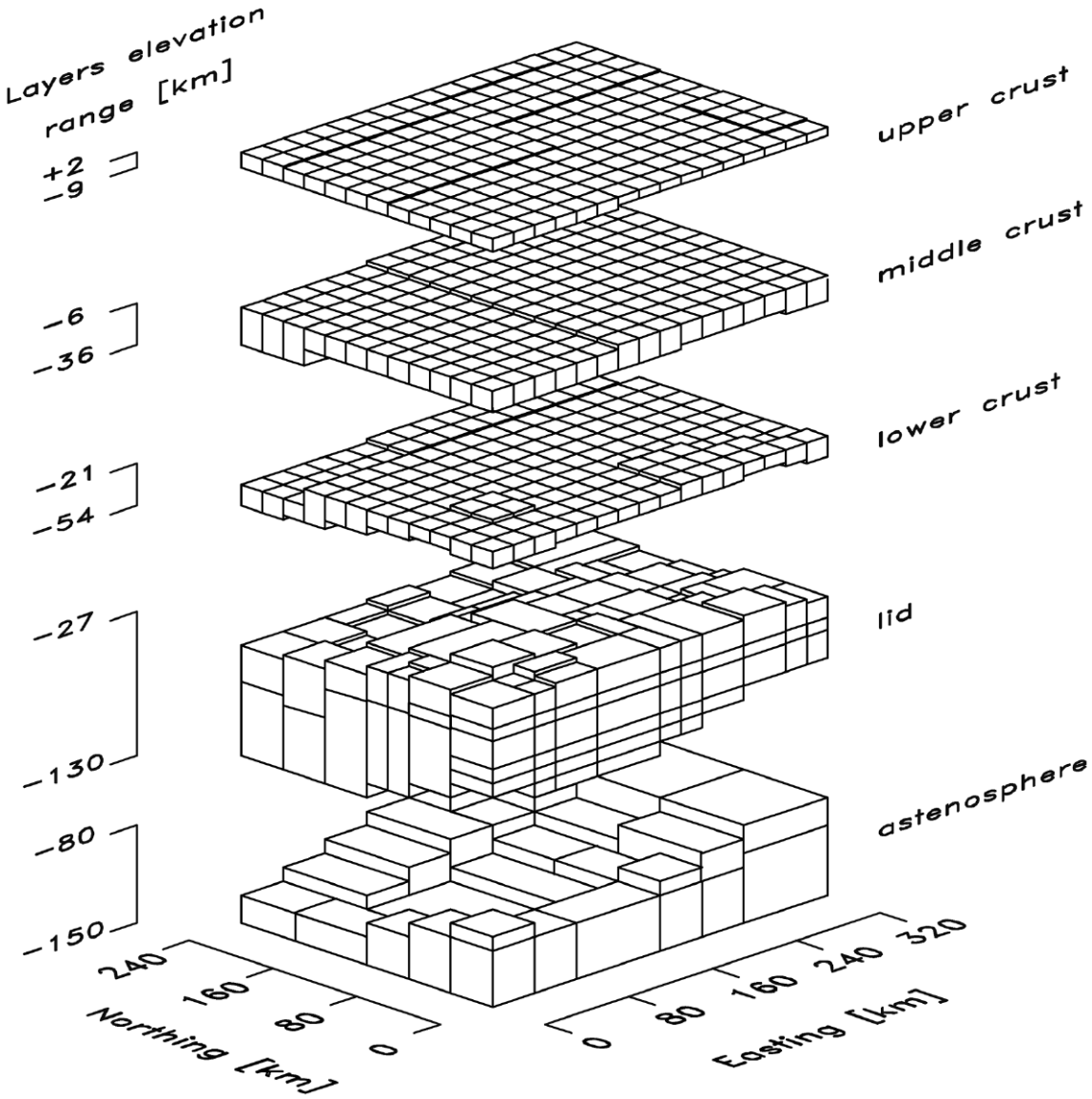

Fig. 2 - The mesh used in the modelling. The lower and upper extremes for each layer are indicated on the side.

middle and upper crust. The depth and shape of the layers' boundaries, as well as their elastic parameters, are inferred from the seismological and gravity data available. The actual topography has been schematically inserted in the uppermost layer of the present model (Fig. 2).

The whole model is subdivided into more than 800 elements. Preliminary runs have been carried out in order to test the reliability of the solution in terms of the grid size in the five layers, and to find the optimal grid size for the present modelling of the regional stress field. According to Zoback (1992), the first-order stress patterns, generally correlated with plate-driving forces, have a lateral extent up to more than fifty times the thickness of the brittle, upper lithosphere. The lithosphere flexure, localised density contrasts, and lateral strength contrasts induce local stress variations, the lateral extent of which may be several times the thickness of the brittle upper lithosphere. Hence, in deciding the grid size within the present model, the scale of the inhomogeneities at the different depths is considered. A coarser mesh is chosen for the asthenosphere and the lid, which are characterised by variations in thickness, with a wavelength much larger than the model itself (Calcagnile and Panza, 1981). The grid size diminishes from the bottom up to the top of the model, reaching a lateral extent of 20 km for the elements of the upper layers. This spacing enables the modelling of the major inhomogeneities of the crust (Fig. 2). To allow, however, a better comparison with the seismological data, an even finer mesh (10 km side) is considered for the crustal strata as well, with a total approximate number of 3000 elements.

Information about the lithospheric structure comes from studies concerning the dispersion of surface waves (Calcagnile and Panza, 1981). Gravity, magnetic and seismic surveys enlightened the shallower crustal structures (Cassano *et al.*, 1986; Škoko *et al.*, 1987, Slejko *et al.*, 1989; Scarascia and Cassinis, 1997). On this basis, the layer boundaries of the model have been constructed, reproducing the main characteristics of the different lithospheric units' topography.

3. Rheology and mechanics

Each of the five homogeneous layers constituting the model is characterised by distinct values of density and Young's modulus, whereas the Poisson ratio is fixed equal to 0.25 for all of them (Table 1).

Density and Young's modulus values in the low velocity channel and the lid are taken according to the global values of the PREM (Dziewonski and Anderson, 1981; Table 1). More detailed information about the density values in the crust comes from the work of Dal Moro *et al.* (1998). Unfortunately, it only provides information about the structure in the south-western

Table 1 - The crustal densities (ρ) chosen for the five layers of the model after the gravimetric modelling (crust) or after PREM (lid and asthenosphere), and Young's modulus (E) for the five layers of the model.

	ρ (g/cm^3)	E (GPa)
upper crust	2.63	55.38
middle crust	2.82	90.38
lower crust	2.99	117.00
lid	3.29	175.50
asthenosphere	3.36	157.00

part of the model, since the seismic data analyzed come from the two Deep Seismic Soundings (DSS) profiles that crossed the region. The first one is a N-S cross section at 11.5° E, from Innsbruck (Austria) to Vicenza (Italy), and the second one is a WNW-ESE section from Innsbruck to Trieste (Italy) (Italian Explosion Seismology Group and Inst. of Geoph. ETH Zürich, 1981; Scarascia and Cassinis, 1997).

In order to check the reliability of the density structure in the rest of the study area, the 2-D Bouguer observed anomalies (Carrozzo *et al.*, 1986; Fig. 3a) are compared with the ones calculated according to the model, following the approach of Marson and Klingelé (1993). The regional pattern of the Bouguer anomalies appears to be well reproduced by the model (Fig. 3b) although some differences still appear in the smaller-scale pattern, e.g. the gravity high in correspondence to the volcanic outcrops to the east of Verona, ascribable both to the high density contrast and to a Moho shallowing (Ebbing *et al.*, 2001; Ebbing, 2004).

4. Forces-displacements modelling

Some boundary conditions are fixed, such as the free surface ones at the upper topographic surface and the conditions of the model bottom, where vertical displacements are set to be null. The remaining ones are conditions that we try to tune, to obtain the best fit with the available observations, i.e. the stress orientations, and the fracturing distribution. The various boundary conditions tested throughout the research depict different scenarios for the kinematics of this collision area.

To simulate the apparent uniaxial compression presently acting in the region, a compression is applied to the model's southern side. The order of magnitude of the compressive stresses applied to the southern side of the various models is 100 MPa. The criterion used to choose the amplitude of the compressive force is to obtain stresses of the order of magnitude of those observed. The few in situ measurements performed in the region show a maximum stress amplitude ranging from 10 to 50 MPa, not far from the values measured in the Alpine region in the past (Hast, 1973; Kohlbeck *et al.*, 1980; Table A1). The values obtained throughout the whole experiment for the elements corresponding to the measurement sites are of the same order of magnitude (10-50 MPa).

The boundary conditions tested throughout the modelling deal with two main problems. The first is the orientation of the forces acting in the region, while the second is how the resulting shortening is accomplished.

The main constraint on the orientation of the compressive force in the study area comes from fault-plane solutions of the events of the Friuli 1976 seismic sequence. As said, there is substantial agreement between focal mechanisms calculated by various authors, all indicating that the region is subject to a N-S to a NNW-SSE directed uniaxial compression (Table 2). We, however, considered also the different orientations of the far-field compression hypothesised by the various authors for the whole Adria region, by applying a N-S, NW-SE and NE-SW oriented compressive force to the southern boundary, while setting to null the displacements in a N-S direction on the northern side. The apparent effect of rotation of the plate is taken into account by linearly varying the force amplitude depending upon the longitude.

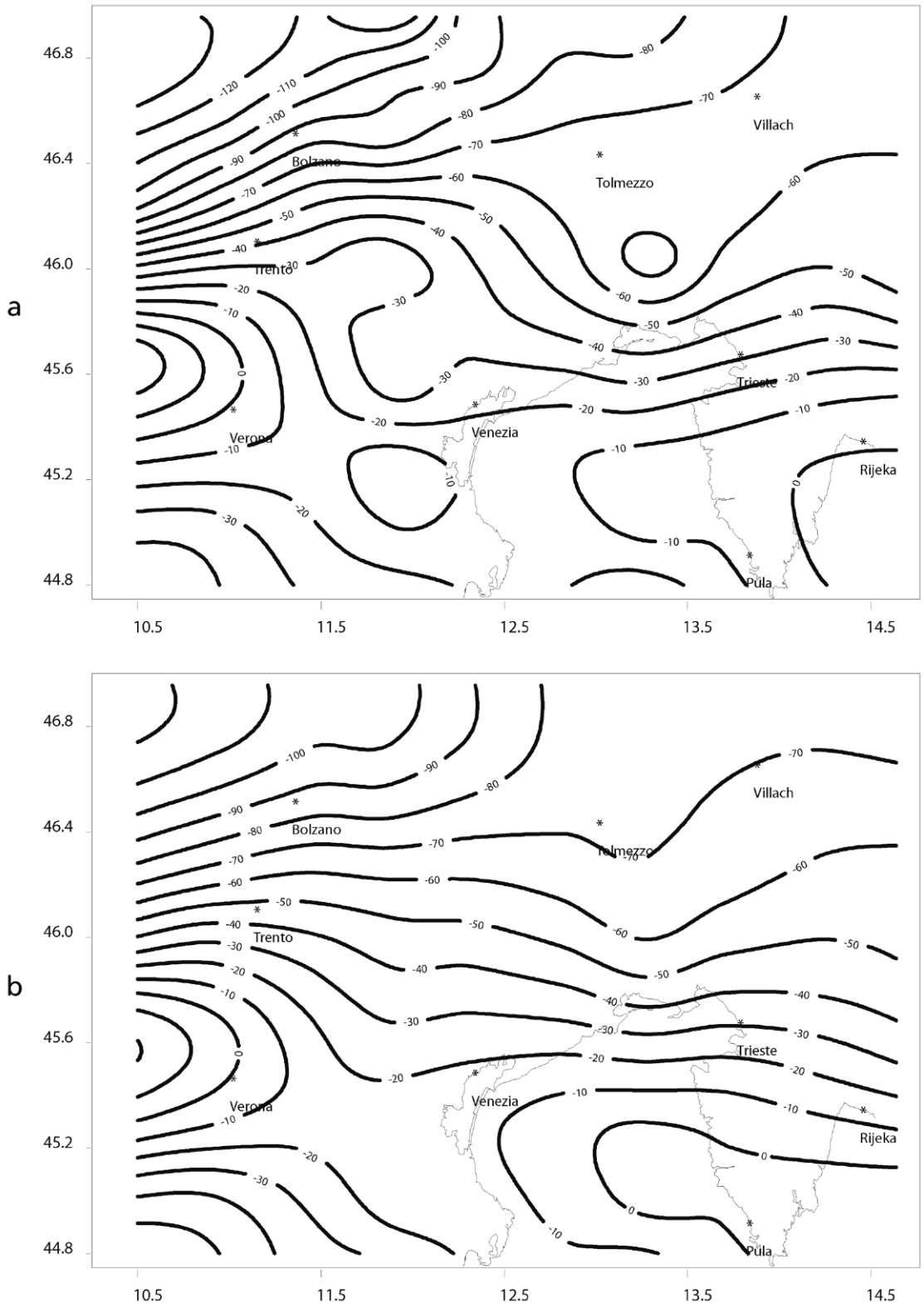

Fig. 3 - Contoured values of the observed (a) Bouguer anomalies (mGal) in the region and calculated (b) for the model.

Table 2 - Fault-plane solutions of the *M*=6.4 Friuli May 6, 1976 earthquake.

	azimuth (°)	dip (°)	rake (°)
Console (1976)	260	14	92
Ebblin (1976)	205	18	39
Müller (1977)	225	10	60
Cipar (1980)	260	15	100
Lyon-Caen (1980)	222	16	52
Suhadolc et al. (1988)	280	30	115
Anderson and Jackson (1987)	267	15	101
Slejko et al. (1989)	230	22	63

The second problem the boundary conditions deal with is given by the modalities of the resulting shortening. There are two alternative ways: mainly by vertical elongation (thrusting), or by horizontal displacements (strike-slip faulting), a third possibility being the intermediate one (Jackson and McKenzie, 1988; England and Jackson, 1989). From the fault-plane solutions evaluated for this area it appears that the latter is prevalent in the study area (Table A1). For this reason, on the lateral sides of the model, the displacements are allowed to occur only in a particular direction, namely, the orientation of the possible shear structures.

Several combinations of the above mentioned boundary conditions have been applied as test to the model, in order to find a solution in good agreement with deformational and seismological data. Summarising, apart from the free surface conditions at the upper surface, and the null vertical displacements at the bottom, the single boundary condition, which is common to all the steps of the experiment, regards the northern boundary of the model, where only E-W displacements are allowed. Displacements are allowed along the lateral sides of the model, but the orientation of the sliding planes varies from model to model. Similarly, also the orientation of the compression applied to the southern side of the model varies, or, as said, its amplitude does.

All the models are tested either in absence of the lithostatic load or considering its effects. As may be expected, its introduction alters the absolute as well as the relative magnitude of the stress principal axes. In the present modelling, however, the change was so small, that the results are practically not affected. In the following, therefore, we consider the deviatoric stress state in the region.

To test the different boundary conditions and models two main criteria are chosen.

A. The first test criterion is the azimuth of the maximum horizontal compression (S_{Hmax}), the most reliable stress parameter calculated from observations (Zoback, 1992).
B. The second criterion is the distribution of seismic activity, and therefore of the areas where the stresses exceed the crustal strength, giving rise to the fracturing, through new faulting, or the re-activation of preceding rupture planes. The distribution of the elastic stress energy within the model, quantified by the second invariant of the stress tensor, function of the relative amplitudes of the principal stresses is analogous.

We present the results of the four models representing the major steps of our analysis (Fig. 4).

The first two models (MOD1 and MOD2) are used to test how the convergence between Europe and Adria (be it an African promontory or an independent block) is accommodated: thrust (MOD1) and a combination of thrust and strike-slip faulting (MOD2). For simplicity, the

convergence is assumed to be N-S oriented. The last two models (MOD3 and MOD4), on the other hand, tested the nature and orientation of such a convergence: NNW-SSW oriented uniform compression (MOD3) or a linearly varying compression with longitude to simulate an apparent counterclockwise rotation (MOD4).

MOD1 - According to the first model (Fig. 4a) the N-S constant convergence is accomplished by vertical elongation of the material comprised between the two plates. The E-W displacements of the elements belonging to the eastern and western sides are also null, to avoid material expansion under compression.

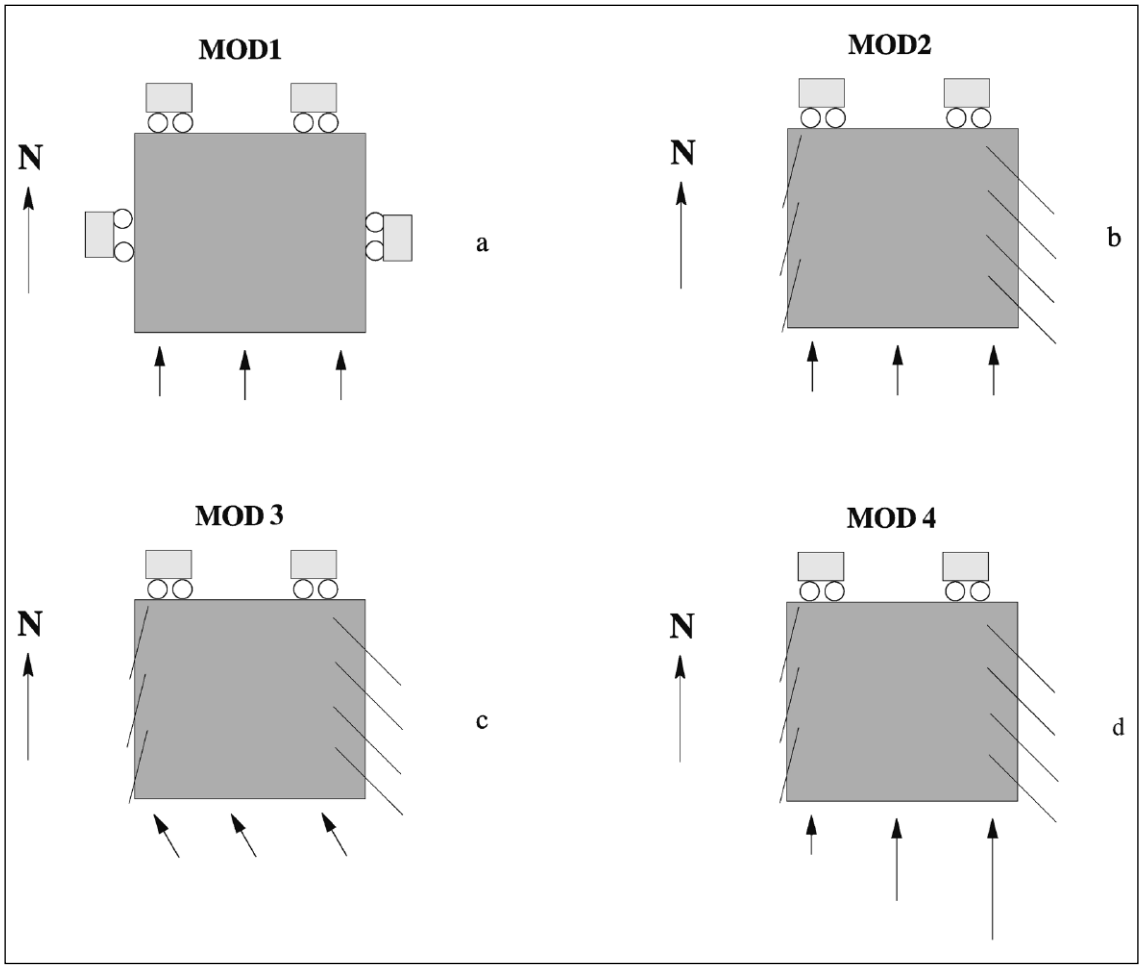

Fig. 4 - The boundary conditions imposed on the three main steps of the analysis. The grey area indicates the modelled region. The thick arrows indicate the compressive forces applied to the southern boundary. Fine-line symbols indicate the orientation of possible sliding planes, taking up part of the deformation. Rolling-bearing symbols indicate the direction of the displacements allowed.
a) MOD1. A constant compressive N-S stress is applied to the southern boundary. The N-S displacements for the nodes on the northern side, as well as the E-W displacements for the nodes belonging to the eastern and westerns sides are null. b) MOD2. A constant compressive N-S stress is applied to the southern boundary. The N-S displacements for the nodes on the northern side are null. The nodes belonging to the eastern and western sides are free to move along planes oriented as the main tectonic discontinuities in the area. c) MOD3. A NNW-SSE oriented compression is applied to the southern side. Other boundary conditions as in b). d) MOD4. A longitude-depending stress is applied to the southern boundary. Other boundary conditions as in b).

MOD2 - The second model (Fig. 4b) allows for the hypothesis that the convergence between the two plates may be accomplished by a combination of thrust and strike-slip faulting. Along eastern and western sides, the model is allowed to slide along the local major tectonic structures. On the western side the orientation is NNE-SSW, parallel to the Giudicarie Line (see Fig. 1b), whereas on the eastern side it is NW-SE, parallel to the Dinaric faults (e.g. the Idrija fault in Fig. 1b). The displacements are null in the direction which is normal to these sliding side planes (NNW-SSE on the western and NE-SW on the eastern one).

MOD3 - The third model (Fig. 4c) differs from the second one only in the orientation of the compressive force acting on the southern side. In agreement with the fault-plane solution proposed for the Friuli 1976 earthquake, it is NNW-SSE oriented.

MOD4 - The fourth model (Fig. 4d) is the most consistent with the seismological evidence, which hypothesizes a counterclockwise rotation of the Adria microplate around a pole located to the west of our study area. Therefore, a compressive stress, linearly increasing to the east, was applied, and a good agreement with observational data was found taking 3 MPa at the south-western corner of the model, and 100 MPa at the south-eastern corner of it.

5. Results

The two test criteria mentioned above mainly involve the first ten kilometres of the crust, where most of the seismic events occur, and where the few direct pieces of information of stress from in situ measurements is available. In the following, the S_{Hmax} trajectories are displayed for the first and third crustal layers of our model, to evaluate the changes induced by the boundary conditions and by the crustal inhomogeneities, more pronounced at the Moho boundary than at shallow depth in the crust. Regarding the second criterion, we calculated the distribution of the second invariant of the stress tensor, indicating the possible fracturing areas for the upper part of the model (first and second crustal layers), where the seismic activity is observed.

5.1. First test criterion: S_{Hmax} orientation

The S_{Hmax} vector calculated in the baricenter of each single element of the upper and lower crustal layers is represented in the following figures.

MOD 1 - In the upper-crust section (Fig. 5a) the stress field is almost homogeneous, showing a slight bend of the S_{Hmax} trajectories in correspondence to the structural high of the Gulf of Venice (Cassano *et al.*, 1986), while the observed divergent compression directions (Fig. 1b) are not evident. The magnitude of the S_{Hmax} is almost homogeneous in this layer, with an increase between 46.2° N and 46.5° N in the piedmont area to the south of the Insubric line. In the lower-crust section (Fig. 5b) the stress field is much more inhomogeneous, both in magnitude and orientation, as expected. The S_{Hmax} trajectories highlight the presence of crustal inhomogeneities. Two main anomalies are evident. The first one is the complex pattern of the stress trajectories in correspondence to the Moho high between Vicenza and Verona, which may coincide with an isotropic point. A second possible isotropic point is evidenced by the drastic re-orientation of the stress trajectories between Tolmezzo and Bolzano, in correspondence to the boundary between the European (about 50 km thick) and the Adriatic crust (around 40 km thick; Scarascia and Cassinis, 1997). A third anomalous zone continues the slight bending of the stress trajectories of

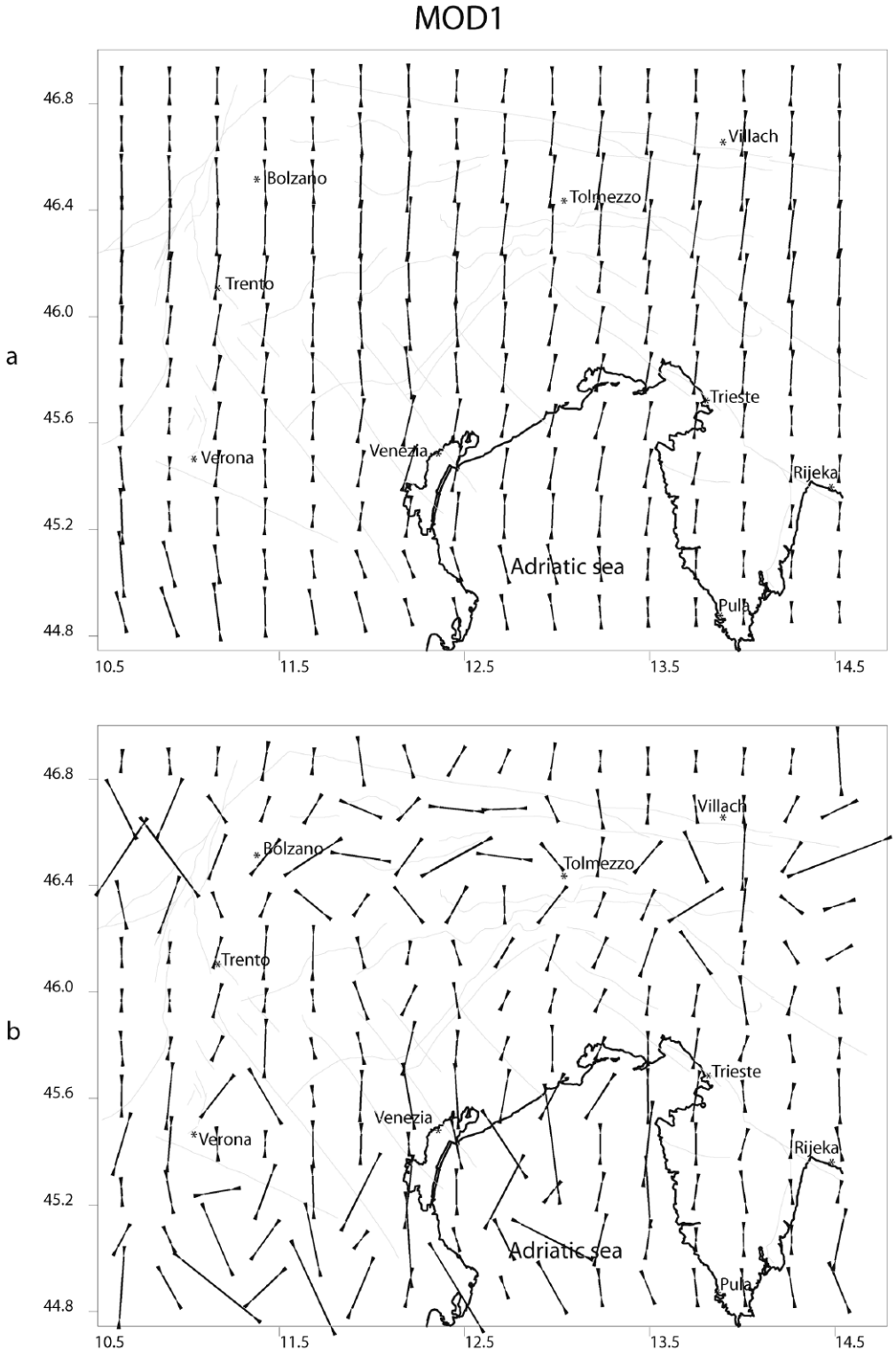

Fig. 5 - MOD1. Projection on the horizontal plane of the maximum compression (S_{Hmax}), calculated in the centroid of each element of the model; the length of the vector is proportional to the S_{Hmax} modulus: a) upper crust; b) lower crust.

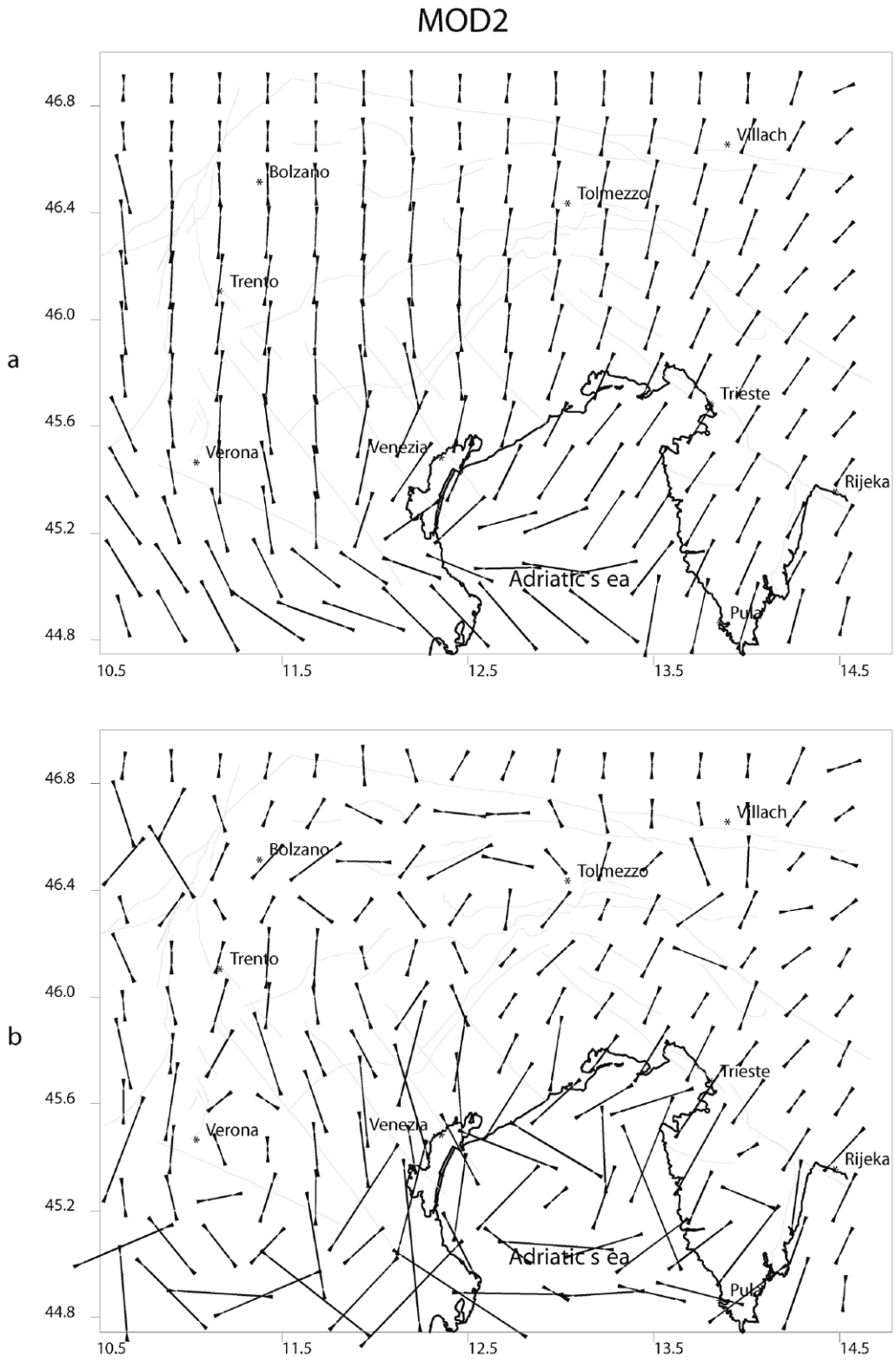

Fig. 6 - As Fig. 6 for MOD2: a) upper crust; b) lower crust.

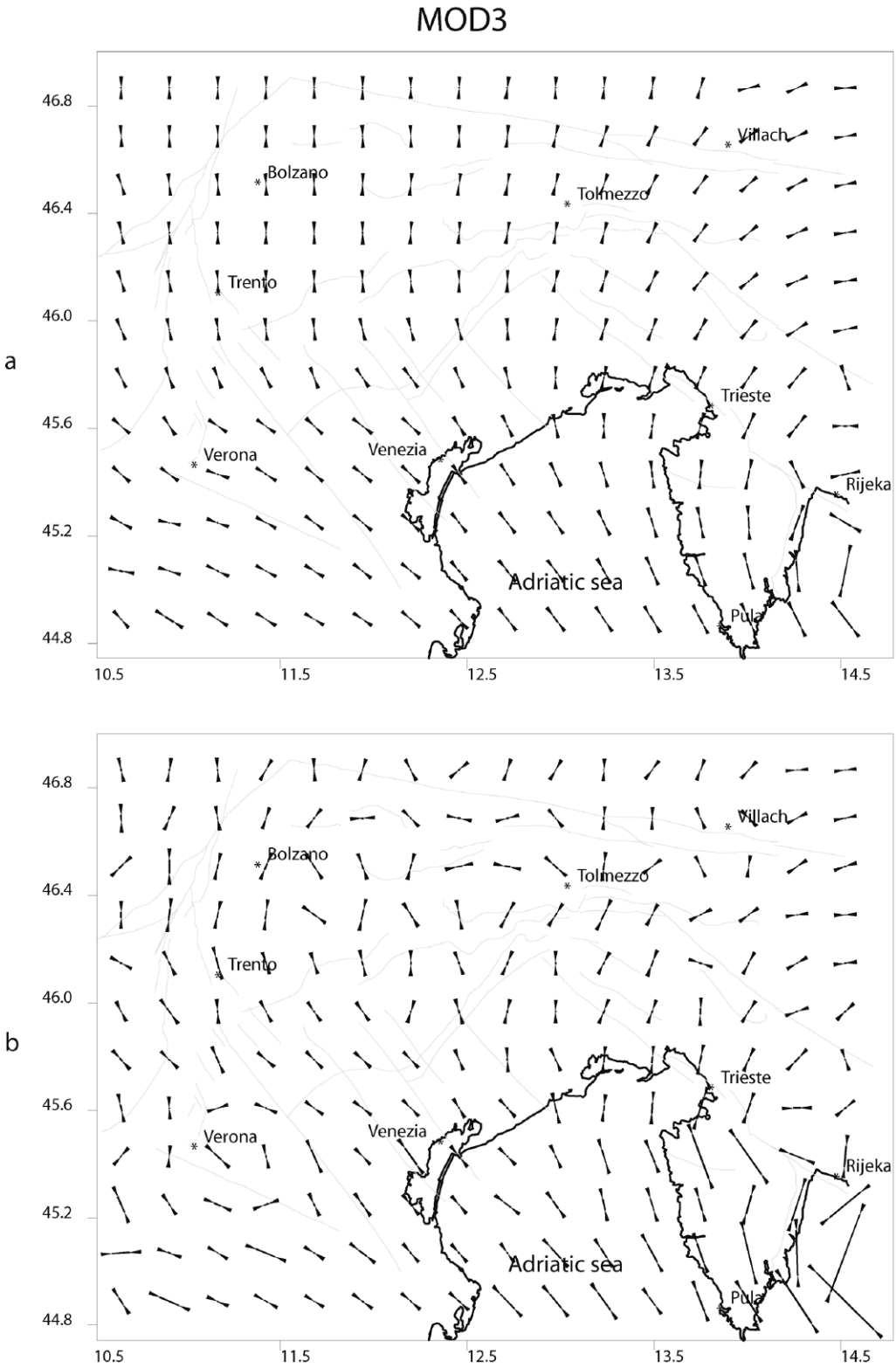

Fig. 7 - As Fig. 6 for MOD3: a) upper crust; b) lower crust.

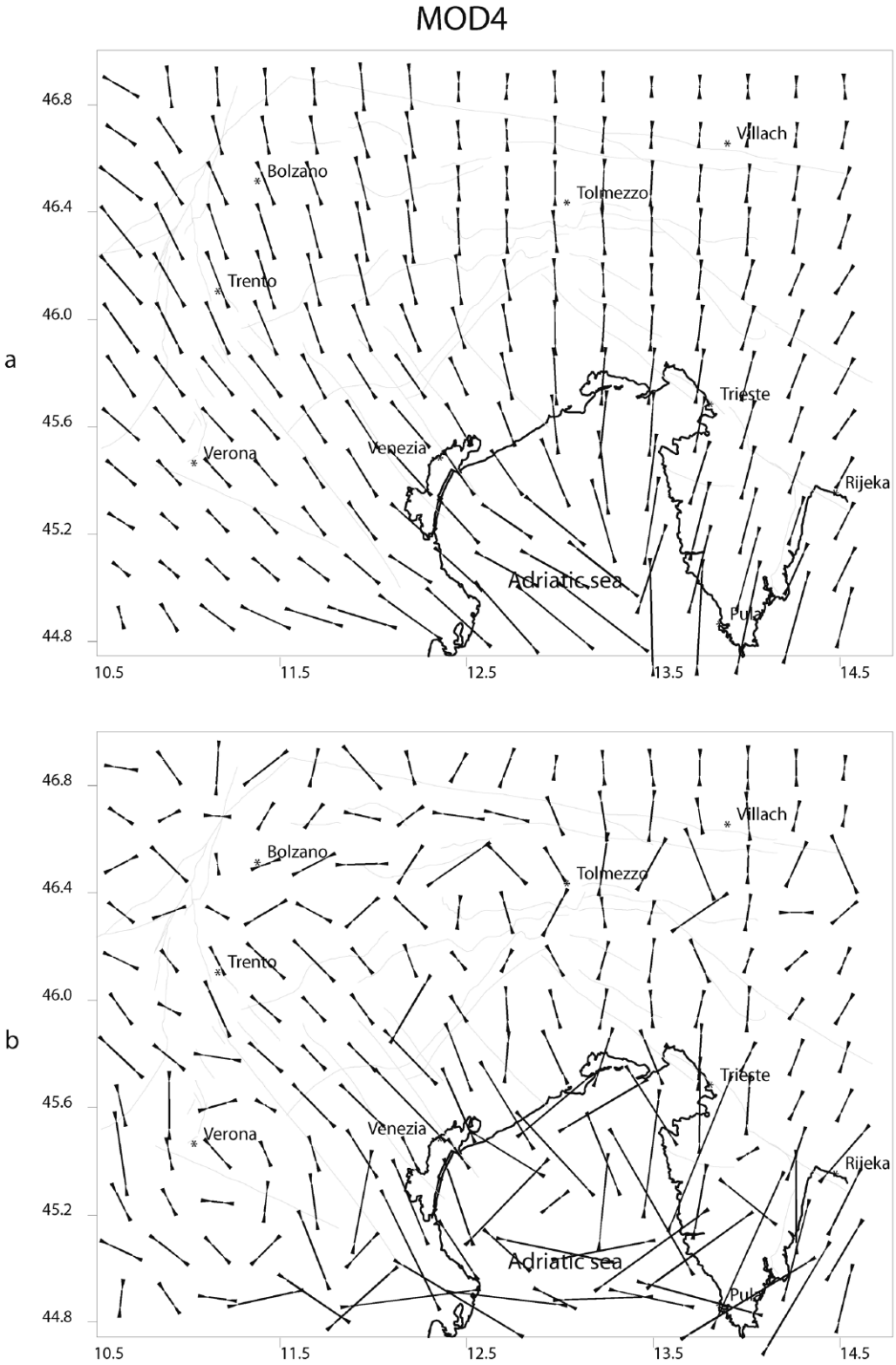

Fig. 8 - As Fig. 6 for MOD4: a) upper crust; b) lower crust.

the upper crust in the Gulf of Venice. Near these three anomalous areas the S_{Hmax} magnitude increases. It also increases between 46.2° N and 46.5° N, in the piedmont area to the south of the Insubric Line.

MOD 2 - The effect of the introduction of the sliding planes parallel to the main observed faults at the lateral borders of the modelled area, is clear in the uppermost section shown in Fig. 6a. The stress trajectories in the eastern part of the model are oriented NE-SW, as from experimental data (Fig. 1b). In the western part of the model, on the contrary, the orientation of the maximum compression is still N-S oriented, instead of the observed NW-SE compression. The zone where these two trends meet, a possible isotropic point is between Verona and Venezia (Venice), and coincide again with the above cited structural high. In the southern part of the model, the S_{Hmax} magnitude varies significantly with respect to the previous case. The lower-crust stress pattern does not change significantly with respect to MOD1 (Fig. 6b), but in the southernmost part of the model. Nevertheless, the three anomalies mentioned above remain unaltered, though also at this depth the stress trajectories in the eastern part of the model are NE-SW oriented (Fig. 6b). The S_{Hmax} amplitude is much higher in the south-easternmost part of the model than in the rest of it.

MOD 3 - The application of a NNW-directed compression produces the divergent pattern of the stress trajectories, more pronounced than the ones observed (Fig. 7a). The compression, NW directed in the southern part of the model, assumes a N-S direction in the north-western part of the model, near Bolzano, which is in disagreement with the observations (Fig. 1b). In the north-eastern part of the model the trajectories vary from NE-SW to almost E-W, thus having a deflection higher than that for real data. A possible isotropic point is in the Istrian Peninsula, or to the east of it. The amplitude is significantly higher in this part than in the piedmont area. In depth (Fig. 7b) like in the preceding cases, the crust inhomogeneities strongly affect the stress trajectories, i.e. in the above-mentioned area of Verona and in correspondence to the boundary between the European and Adriatic crusts. The amplitude is much higher in the south-easternmost part of the model than in the rest of it.

MOD 4 - The introduction of the linear increase of compression with longitude also affects the orientation of the stress trajectories. The stress pattern agrees with the divergent compression directions observed (Fig. 8a). The stress trajectories are about N-S in the Friuli seismic area, whereas they show a NE-SW pattern in the Istrian Peninsula and to the east of Trieste, as observed in the focal mechanisms. To the west of Venezia they assume a clear NW-SE orientation. The point where the two orientations converge, a possible isotropic point, is off the Istrian peninsula, where a relevant Bouguer anomaly is observed (Italian Explosion Seismology Group and Inst. of Geoph. ETH Zürich, 1981; see Fig. 3a), related to a high of the Moho. The S_{Hmax} amplitudes are higher in this region of the model than in the rest. Another increase is localized between Bolzano and Tolmezzo in the piedmont area. In depth (Fig. 8b) like in the preceding cases, the crust inhomogeneities strongly affect the stress trajectories, i.e. in the above-mentioned area of Verona, Gulf of Venice, and in correspondence to the boundary between the European and Adriatic crusts. As in the second model, the S_{Hmax} amplitude is higher in the southernmost part of the model, and again in the piedmont area, with the highest relative values near Tolmezzo.

A divergent pattern of compression trajectories, like the observed one, is obtained both with

MOD3 and MOD4. It is the latter, however, that shows a better fit with the observations, and appears, therefore, more reliable.

5.2. Second test criterion: faulting and fracturing

The distribution of the seismic events shows where the tectonic stresses exceed the strength of the crust, to produce or re-activate fracturing. A quantity, which is directly comparable with the results of a modelling like the present one, is the seismic energy E_s:

$$\log E_s = 1.5\, M + c \qquad (1)$$

where M is the magnitude of the event, and c is a constant (Kanamori and Anderson, 1975).

Its distribution can be compared with the distribution of the elastic stress energy within the model. This quantity may be represented by the second invariant of the stress deviator I_2:

$$I_2 = (\sigma_1 - \sigma_2)^2 + (\sigma_2 - \sigma_3)^2 + (\sigma_3 - \sigma_1)^2 \qquad (2)$$

function, therefore, of the relative amplitudes of the three principal stresses $(\sigma_1, \sigma_2, \sigma_3)$. I_2 is the yield criterion according to von Mises (Jäger, 1962, p. 27).

The seismic energy released in the region as recorded in about twenty years of observations (1977-2001) by the north-eastern Italy seismometric network (Slejko *et al.*, 1989; OGS, 1977-2001) is mapped in Fig. 9a, together with the epicentres of the events considered. Only events with magnitude greater than 2.5 are considered, to deal with catalogue completeness (e.g. Braitenberg, 2000). The highest values are recorded near Tolmezzo, where the aftershock activity of the 1976 earthquake was concentrated, and the more intense seismic activity is still recorded, notwithstanding the recent intense activity near Bovec. The epicentres are sparse along the curved piedmont area, and small clusters are observed outside these areas, as for example near Trento.

The values of I_2 are calculated for the elements of the upper crust, i.e. the seismogenic layer (Slejko *et al.*, 1989), and are mapped in Fig. 9b for MOD3 and in Fig. 9c for MOD4.

The much better fit of MOD4 with respect to MOD3 is striking. In the first case the highest values of I_2 are concentrated in the area near Tolmezzo, quite close to the area where the highest seismic energy values are observed, and where the May 6, 1976, M=6.4 earthquake occurred. In the case of MOD3, on the contrary, the highest values are concentrated to the west of it, where there is seismic activity, but not so intense. Analogous tests made for MOD1, MOD2, and the other steps of the experiment show a much poorer fit with the observed data than MOD4.

MOD4 does not fit all the characteristics of the fracturing distribution. The model does not reproduce, for example, the small cluster of seismic activity observed near Trento in the western part of the region. This sequence is characterised by low magnitudes, and is generally interpreted as the manifestation of the activity of a small local structure (Slejko *et al.*, 1989), so hardly reproducible by a model as the present one. It could, however, also mean that some additional refinement is still required at the north-western corner of the model. The good fit in the Friuli seismic area and along the Dinarides confirms, however, the general validity of the present modelling.

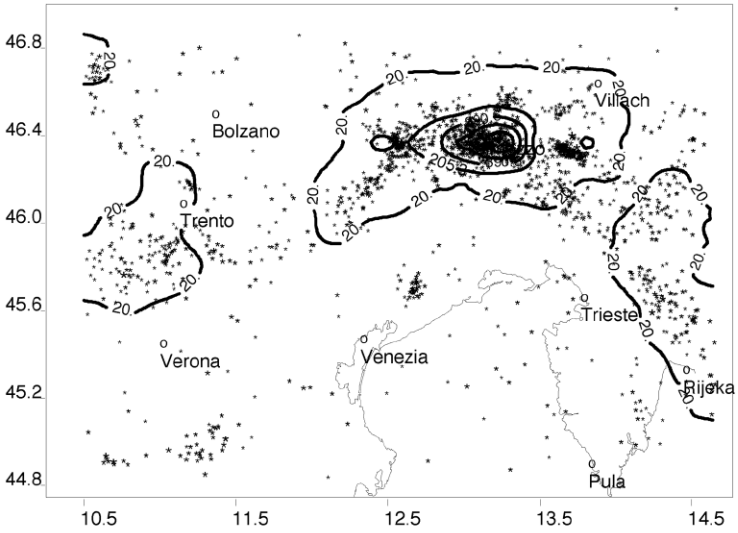

Fig. 9 - a) Contoured values of the seismic energy released from 1977 to 2001 in the region and epicenter locations (O.G.S. 1977-2001). b) Contoured values of the second invariant of the deviatoric stress, failure threshold according to von Mises's criterion, calculated as mean value for the elements of the upper-crust layer of MOD3. c) As b) for MOD4.

6. Discussion and conclusions

Modelling results, and in particular, MOD4 results, show a good agreement with the available information about the stress-strain field at the north-eastern boundary of the Adria microplate. Before going in more details about the possible implications of these results, the assumptions and the possible limits of the present modelling will be discussed shortly.

First of all, as said, this one is an elastic, static model of the actual stress field, built up on the basis of the information about the present geometry and structure of the different lithospheric units. The last ones are the result of a long series of tectonic events and processes, whose modelling is a very interesting research field, that however goes beyond the goals of the present work. Moreover, the limited extents of the considered area implies that processes that occur at the model's boundary, as for example the stress regime close to the Apennines, cannot be properly modelled.

On the contrary, for the region of our interest, the modelling reproduces the pattern of the compression trajectories of the region pretty well. And this, notwithstanding the unavoidable simplification adopted in reproducing the geometry of the different lithospheric units. This agreement confirms the validity of the criteria chosen to discretize the region, based on the scale of the inhomogeneities at the different depths and, therefore, on the scale of the plausible deviations of stress trajectories (Zoback, 1992). Another validation of the geometric characteristics of the model is given by the comparison between the observed Bouguer anomalies and the ones calculated on the basis of the model itself. The general pattern is well reproduced, while small discrepancies are mainly due to the shallow density anomalies, not reproduced in the model.

The last confirmation of the validity of the model as a study tool for the seismotectonic phenomena in the region, comes from the comparison between the seismic energy and the elastic stress energy distributions. In addition to the von Mises fracturing criterion, the other fracturing criteria (as e.g. Tresca criterion) have also been tested, and their results are similar to the ones presented here. The choice of this one in particular was, however, suggested by the possibility of a direct comparison between two analogous physical quantities: seismic energy and elastic energy, quantified by the second invariant of the stress tensor, I_2, which is not possible adopting other fracturing criteria.

The agreement between the two distributions (i.e. seismic energy and I_2) for MOD4 is really impressive, overall when compared with the results from MOD3. It has to be, however, recalled, that, because of the uncertainty about the real stress amplitude in the region, I_2 distribution is only indicative of the areas where, under the far-field compression and the boundary conditions imposed on the models, the strength of the crust masses is exceeded. To state the amplitude of the compression to be applied at the model's southern side, the few available data regarding the tectonic stress amplitude in the region, were used. These data show that the maximum amplitude varies between 10 and 50 MPa, values not far from those recorded in other areas of the Alpine region (Hast, 1973; Kohlbeck *et al.*, 1980). The values obtained from the whole modelling in correspondence with measurement locations are of the same order of magnitude, in the presence, as well as in the absence, of the lithostatic load, but it would be far better to have additional direct measurements to which to anchor the modelling. The last uncertainty about MOD4, in particular,

is the linear increase with longitude attributed to the compression at the model's southern side. This linear law has been chosen as a first approximation of the effects of a counterclockwise rotation of Adria with respect to Eurasia, around a pole located to the west of the study area.

In addition to the four steps presented here, other kinematic hypotheses have been tested. It is noteworthy, that testing other orientations of the compression acting at the southern side, in agreement with the hypotheses of Ward (1994) or Albarello *et al.* (1995), we never obtained a fitting of the observed data comparable with the ones of MOD4.

The stress field pattern observed may be explained as an effect of the counterclockwise rotation of the Adria microplate around a pole located to the west of the study area, in agreement with seismological and geodetic data (Anderson and Jackson 1987; Westaway, 1990; Ward, 1994). The consequent shortening is partly achieved through thrusting, partly through strike-slip faulting at the lateral sides.

The mechanisms that rule continental collision, like the one that is still acting in the study area, are still doubtful and being debated. As pointed out by Jackson and McKenzie (1988), the vertical elongation of the material comprised between the two plates (thrusting) and lateral extrusion along a direction normal to the relative motion vector (strike-slip faulting) may act both separately, or also, simultaneously. In particular, according to England and Jackson (1989), after the early stage of vertical thickening, crustal buoyancy inhibits further thickening, so that part of the convergence may be taken up by strike-slip. It is a very plausible scenario for a region that records the maximum crustal thickening of the Alps (Castellarin, 1979; Laubscher, 1990; Castellarin *et al.*, 1992). Moreover, strike-slip faulting mechanisms are observed just in the western and easternmost areas (Dinarides and the area around the Garda Lake: Slejko *et al.*, 1989; Carulli *et al.*, 1990; Bressan *et al.*, 1998; 2003; Table A1). It is noteworthy that the introduction of sliding planes at the eastern side, with a Dinaric trend may also be seen in terms of additional forces, NE-SW directed, from the lateral boundaries. This would mean that there is an active role of the Dinaric front in the tectonics of the region, as hypothesised in other studies (Castellarin *et al.*, 1992).

Another explanation for the observed pattern is, however, possible. A similar radial pattern of the compression trajectories is recorded also in the western Alps, normally towards the mountain belt. It can be explained as being due to the complex processes of indentation and rotation of lithospheric blocks (Vialon *et al.*, 1989), or to a relevant thickening of the lithosphere (Fleitout and Froidevaux, 1982; Grünthal and Stromeyer, 1992). The negative buoyancy of the latter may overcome the tension due to the high topography, and may be responsible for additional compression (Zoback, 1992). In the study area, however, both elevation and lithospheric thickness are reduced with respect to the western Alps, and therefore, their effect on the stress field, should be smaller as well. The present modelling deals with the effects of the topography, of the lithostatic load and of the stiffness contrast between the different lithospheric units. Buoyancy is presently not included, but will be taken into account in the next refinements of the model. It is, in fact, possible that different mechanisms all contribute to the overall deformation in the complex process that is the continental collision, as demonstrated for the back-arc extension case by experimental modelling (Faccenna *et al.*, 1996).

The elastic case presented here represents only a first approximation of the stress-strain

conditions in the region. In the near future the model will be in fact extended to the dynamic, viscous-elastic case. With all its limits, however, this model represents a precious tool to simulate and study the present stress-strain field characteristics in the region, and provide a possible interpretation in the frame of the regional kinematics, while testing the different geodynamic hypotheses.

Acknowledgements. We thank Giancarlo Dal Moro, Iginio Marson and Isabella Velicogna for their helpful discussions and contribution to the gravity test of the model. We thank Gianni Bressan and Carla Braitenberg for the fruitful and constructive comments that helped us to improve our paper. We also thank the Istituto Nazionale di Oceanografia e di Geofisica Sperimentale-OGS, Trieste (Italy), for having put at our disposal the N.E. Italy local seismometric network data for comparison with our results. This research was supported with the MURST funds (Contractor M. Zadro); 40% R.95 02/09/02 -A227; 60% R95. 02/02/01-A068, the CNR funds (Contractor M. Zadro) 95.00339.CD05 02/09/05-327, and EC research grant IC15CT96-0205 (Contractor M. Zadro). Part of the results of this research were presented at the 2nd Int. Symposium: Geodynamics of Alps-Adria area by means of terrestrial and satellite methods, Dubrovnik, Sept. 28 - Oct 2 1998.

REFERENCES

Albarello D., Mantovani E., Babbucci D. and Tamburelli C.; 1995: *Africa-Eurasia kinematics: main constraint and uncertainties*. Tectonophysics, **143**, 25-36.

Altiner Y.; 1999: *Analytical surface deformation theory for detection of the Earth's crust movements*. Springer, Heidelberg, 110 pp.

Anderson H. and Jackson J.; 1987: *Active tectonics of the Adriatic region*. Geophys. J. R. astron. Soc., **91**, 937-983.

Argand E.; 1924: *La tectonique de l'Asie*. In: Proc. Int. Geol. Congr., XIII, pp. 171-372.

Barbano M.S., Kind R. and Zonno G.; 1984: *Focal parameters of some Friuli earthquakes (1976 - 1979) using complete theoretical seismograms*. J. Geophys., **58**, 175-182.

Bassi G., Sabadini R. and Rebai S.; 1997: *Modern tectonic regime in the Tyrrhenian area: observations and models*. Geophys. J. Int., **129**, 330-346.

Braitenberg C.; 1999: *The Friuli (NE-Italy) tilt/strain gauges and short term observations*. Annali di Geofisica, **42**, 1-28.

Braitenberg C.; 2000: *Non-random spectral comoponents in the seismicity of NE-Italy*. Earth Planet Science Letters, **179/2**, 379-390.

Braitenberg C., Nagy I., Negusini M., Romagnoli C., Zadro M. and Zerbini S.; 2001: *Geodetic measurements at the northern border of the Adria plate*. Journal of Geodynamics, **32**, 267-286.

Bressan G., Snidarcig A. and Venturini C.; 1998: *Present state of tectonic stress of the Friuli area (eastern Southern Alps)*. Tectonophysics, **292**, 211-227.

Bressan G., Bragato P.L. and Venturini C.; 2003: *Stress and strain tensors based on focal mechanisms in the seismotectonic framework of the Friuli-Venezia Giulia Region (Northeastern Italy)*. Bull. Seism. Soc. Am., **93**, 1280-1297.

Calcagnile G. and Panza G.F.; 1981: *The main characteristics of the lithosphere-asthenosphere system in Italy and surrounding regions*. Pure appl. Geophys., **119**, 865-879.

Carrozzo M.T., Luzio D., Margiotta C. and Quarta T.; 1986: *Gravity map of Italy*. CNR, Progetto finalizzato Geodinamica.

Carulli G.B., Nicolich R., Rebez A. and Slejko D.; 1990: *Seismotectonics of the northwest external Dinarides.* Tectonophysics, **179**, 11-25.

Cassano E., Anelli L., Fichera R. and Cappelli V.; 1986: *Pianura Padana: interpretazione integrata di dati geologici e geofisici*. In: 73° Congr. Soc. Geol. It., AGIP; pp. 1-28.

Castellarin A.; 1979: *Il problema dei raccorciamenti crostali nel sudalpino*. Rend. Soc. Geol. It., **1**, 21-23.

Castellarin A., Cantelli L., Fesce A.M., Mercier J.L., Picotti V., Pini G.A., Prosser G. and Selli L.; 1992: *Alpine compressional tectonics in the Southern Alps. Relationship with the N-Apennines*. Ann. Tectonicae, **6/1**, 62-94.

Cipar J.; 1980: *Teleseismic observations of the Friuli, Italy earthquake sequence*. Bull. Seism. Soc. Am., **70**, 963-983.

Console R.; 1976: *Focal mechanism of some Friuli earthquakes (1976)*. Boll. Geof. Teor. Appl, **19**, 549-558.

Dal Moro G., Braitenberg C. and Zadro M.; 1998: *Geometry and mechanical crustal properties in NE Italy based on seismic and gravity data*. Boll. Geof. Teor. Appl., **39**, 37-46.

Dziewonski A.M. and Anderson D.L.; 1981: *Preliminary reference model*. Phys. of the Earth and Plan. Int., **25**, 297-356.

Ebbing J.; 2004: *The crustal structure of the Eastern Alps from a combination of 3D gravity modelling and isostatic investigations*. Tectonophysics, **380**, 89-104.

Ebbing J., Braitenberg C. and Götze H.-J.; 2001: *Forward and inverse modelling of gravity revealing insight into crustal structures of the Eastern Alps*. Tectonophysics, **337**, 191-208.

Ebblin C.; 1976: *Orientations of stresses and strains in the piedmont area of eastern Friuli*. Boll. Geof. Teor. Appl., **19**, 559-579.

Ebblin C.; 1980: *Fault-plane solutions and hypocentral distribution of some 1977 Friuli aftershocks*. Geophys. J.R. astron. Soc., **62**, 97-12.

Ebblin C.; 1986: *First estimates of the principal directions of strain compared with those of stresses in seismic Friuli, NE Italy*. Pure Appl. Geophys., **124**, 897-917.

England P. and Jackson J.; 1989: *Active deformation of the continents*. Am. Rev. Earth Planet. Sci., **17**, 197-226.

Faccenna C., Davy P., Brun J-P., Funiciello R., Giardini D., Mattei M. and Nalpas T.; 1996: *The dynamics of back-arc extension: an experimental approach to the opening of the Tyrrhenian Sea*. Geophys. J. Int., **126**, 781-795.

Fleitout L. and Froidevaux C.; 1982: *Tectonics and tomography for a lithosphere containing density heterogeneities.* Tectonics, **1**, 21-56.

Grünthal G. and Stromeyer D.; 1992: *The recent crustal stress field in Central Europe: trajectories and finite element modelling*. J. Geophys. Res., **97**, 11805-11820.

Hast N.; 1973: *Global measurements of absolute stress*. Phil. Trans. R. Soc. London, **274**, 409-419.

Horváth F.; 1984: *Neotectonics of the Pannonian basin and the surrounding mountain belts: Alps, Carpathians and Dinarides*. Ann. Geophysicae, **2/2**, 147-154.

Italian Explosion Seismology Group and Inst. of Geoph., ETH, Zürich; 1981: *Crust and upper mantle structures in the southern Alps, from deep seismic soundings profiles (1977-1978) and surface wave dispersion analysis*. Boll. Geof. Teor. Appl., **92**, 297-330.

Jackson J. and McKenzie D. P.; 1988: *The relationship between plate motions and the seismic moment tensors, and the rates of active deformation in the Mediterranean and Middle East*. Geophys. J. R. astron. Soc., **93**, 45-73.

Jäger J.C.; 1962: *Elasticity, fracture and flow*. Methuen & Co., London, 208 pp.

Kanamori H. and Anderson D.L.; 1975: *Theoretical basis of some empirical relations in seismology*. Bull. Seism. Soc. Am., **65**, 1073-1095.

Kohlbeck F., Rock K-H. and Scheidegger A.E.; 1980: *In situ stress measurements in Austria*. Rock mechan. Suppl., **9**, 21-29.

Kravanja S., Costa G., Panza G.F. and Suhadolc P. 1999: *Full moment tensor retrieval from waveform inversion: an application to the Bovec event (Slovenia) and its swarm*. In: EGS XXIV Gen. Assembly, The Hague, The Netherlands, 19-23 April, 1999.

Laubscher H.P.; 1990: *The problem of the deep structure of the Southern Alps: 3-D material balance considerations and regional consequences*. Tectonophysics, **176**, 103-121.

Lyon-Caen H.; 1980: *Seismes du Frioul (1976): modelles de source a l'aide de sismogrammes synthetiques d'ondes de volume*. PhD. Thesis, Université Paris VII.

Mao W.J., Ebblin C. and Zadro M.; 1989: *Evidence for variations of mechanical properties in the Friuli area*. Tectonophysics, **170**, 231-242.

Mao W. J., Santero P. and Zadro M.; 1990: *Long- and middle-term behaviour of the tilt and strain variations in the decade following the 1976 earthquake in NE-Italy*. Pure Appl. Geophys., **132**, 653-677.

Marson I. and Klingelé E.E.; 1993: *Advantages of using the vertical gradient of gravity for 3-D interpretation*. Geophysics, **58**, 1588-1595.

Marussi A.; 1959: *The University of Trieste station for the study of the tides in the vertical in the Grotta Gigante*. In: Proceedings of the Third International Symposium on Earth Tides, Pubbl. 49, Ist. di Topog. e Geodesia, Univ. Trieste, Trieste, pp. 45-52.

Mayer-Rosa D., Pavoni N., Graf R. and Rast B.; 1976: *Investigations on intensities, aftershock statistics and focal mechanisms of Friuli earthquakes in 1975 and 1976*. Pageoph., **114**, 1095-1103.

Müller G.; 1977: *Fault-plane solutions of earthquake in Northern Italy, 6 May 1976, and implications for the tectonics of Eastern Alps*. J. Geophys., **42**, 343-349.

Müller B., Wehrle V. and Fuchs K.; 1997: *The 1997 release of the World Stress Map* (available on-line at http://www-wsm.physik.uni-karlsruhe.de/pub/Rel97/wsm97.html).

O.G.S.; 1977-2001: Bollettino della Rete sismometrica dell'Italia Nord-Orientale, OGS, Trieste.

Pondrelli S., Morelli A. and Boschi E.; 1995: *Seismic deformation in the Mediterranean area estimated by moment tensor summation*. Geophys. J. Int., **122**, 938-952.

Pondrelli S., Ekstrom G. and Morelli A.; 2001: *Seismotectonic re-evaluation of the 1976 Friuli, Italy, seismic sequence*. J. of Seismology, **5**, 73-85.

Reches Z., Schubert G. and Anderson C.; 1994: *Modeling of periodic great earthquakes on the San Andreas Fault: effects on non linear crustal rheology*. J. Geophys. Res., **99**, 21983-22000.

Rossi G., and Zadro M.; 1996: *Long-term crustal deformations in NE-Italy revealed by tilt-strain gauges*. Phys. of the Earth and Plan. Int., **97**, 55-70.

Rossi G., Zadro M. and Ebblin C.; 1999: *Geodynamic processes at the northern boundary of the Adria microplate: tilt-strain measurements and modelling*. In: Colič K. and Moritz H. (eds), Proc. II Int. Symposium: Geodynamics of Alps-Adria Area by means of terrestrial and satellite methods, Dubrovnik, Sept. 28-Oct 2 1998, Zagreb, 1999, pp. 271-282.

Scarascia S. and Cassinis R.; 1997: *Crustal structures in the Central-Eastern Alpine sector: a revision of the available DSS data*. Tectonophysics, **271**, 157-188.

Škoko D., Prelogovic E. and Alinovic B.; 1987: *Geological structure of the Earth's crust above the Moho discontinuity in Yugoslavia*. Geophys. J. R. astron. Soc., **89**, 379-382.

Slejko D., Carulli G.B., Nicolich R., Rebez A., Zanferrari A., Cavallin A., Doglioni C., Castaldini F., Iliceto V., Semenza E. and Zanolla C.; 1989: *Seismotectonic of the Eastern Southern Alps: a review*. Boll. Geof. Teor. Appl., **31**, 109-136.

Slejko D., Neri G., Orozova I., Renner G. and Wyss M.; 1999: *Stress field in Friuli (NE Italy) from fault plane solutions of activity following the 1976 main shock*. Bull. Seism. Soc. Am., **89**, 1037-1052.

Suhadolc P., Cernobori L., Pazzi G. and Panza G.F.; 1988: *Synthetic isoseismals: applications to Italian earthquakes*. In: Bonnin J. *et al.* (eds), Seismic Hazard in Mediterranean Regions, Kluwer, Dordrecht, Holland, pp. 105-128.

Suhadolc P.; 1990: *Fault-plane solutions and seismicity around the VI EGT*. In: Freeman R. e Müller St. (ed), VI EGT Workshop: Data compilations and Synoptic interpretation, Eur. Science Foundation, Strasbourg, pp. 371-382.

Vialon P., Rochette P. and Menard G.; 1989: *Indentation and rotation in the western Alpine arc*. In: Coward H.P., Dietrich D. and Park R.G. (eds), Alpine tectonics, Geol. Soc., Blackwell Scient. Publ., Oxford, pp. 329-338.

Ward S.N.; 1994: *Constraints on the seismotectonics of the central Mediterranean from very long baseline interferometry*. Geophys. J. Int., **117**, 441-452.

Westaway R.; 1990: *Present-day kinematics of the plate boundary zone between Africa and Europe, from the Azores to the Aegean*. Earth Plan. Sc. Lett., **96**, 393-406.

Zadro M.; 1978: *Use of tiltmeters for the detection of forerunning events in seismic areas*. Boll. Geod. Sci. Aff., **37**, 597-618.

Zadro M. and Braitenberg C.; 1999: *Measurements and interpretations of tilt-strain gauges in seismically active areas*. Earth Science Reviews, **47**, 151-187.

Zoback M.L.; 1992: *First- and second-order patterns of stress in the lithosphere: the World Stress Map Project*. J. Geophys. Res., **97**, 11703-11728.

Appendix

In the frame of the World Stress Map Project (WSMP), the fault-plane solutions calculated by the different authors were revised, and completed with the information from the few in situ stress measurements available, to constitute a precious database (Grünthal and Stromeyer, 1992; Zoback, 1992; Mueller *et al.*, 1997). Table A1 summarises the information on stress orientation that was used in this work. The data are mainly from the WSMP database, and some data from Suhadolc (1990) complete the information for the westernmost part of the study area.

Table A1 - Stress-orientation data from focal mechanisms (FMS) and in-situ measurements (OC). σ1 az = azimuth of the first principal stress axis; σ1 pl = plunge of the first principal stress axis; A1 = absolute amplitude of the first principal stress axis; M = magnitude of the event; type = kind of measurement (FMS or OC); Q = quality according to WSMP standard; ref = reference: 1 = WSMP database (Müller, 1997); 2 = Suhadolc (1990).

date	time	lat.	long.	depth km	σ1 az	σ1 pl	σ2 az	σ2 pl	σ3 az	σ3 pl	A1 MPa	A2 MPa	A3 MPa	M	type	Q	ref
280327	08:32:31.	46.42	13.03	20.00	351	4	86	52	258	38	—	—	—	5.8	FMS	D	1
340608	03:19:09.	46.30	12.50	20.00	160	1	295	89	70	1	—	—	—	4.5	FMS	C	1
341130	02:58:19.	44.10	14.00	30.00	343	17	205	68	77	14	—	—	—	5.6	FMS	D	1
361019	07:05:54.	46.00	12.50	10.00	159	1	294	89	69	1	—	—	—	4.5	FMS	D	1
361018	03:10:12.	46.10	12.46	17.00	157	28	310	59	61	12	—	—	—	5.6	FMS	C	1
390211	11:16:00.	44.07	11.65	7.00	150	74	332	17	241	1	—	—	—	4.7	FMS	C	1
391015	15:05:00.	44.23	10.20	27.00	331	62	210	16	113	23	—	—	—	4.9	FMS	C	1
561105	19:45:25.	46.56	12.96	2.00	316	7	185	79	47	8	—	—	—	4.8	FMS	C	1
590426	14:45:16.	46.47	13.00	5.00	168	23	338	67	75	3	—	—	—	4.4	FMS	C	1
630519	10:00:08.	46.27	14.53	13.00	33	15	123	1	217	75	—	—	—	5.3	FMS	C	1
670512	17:53:00.	44.76	10.67	39.00	347	67	226	13	131	19	—	—	—	4.2	FMS	D	1
670814	10:16:18.	46.90	10.40	11.00	354	8	261	16	108	71	—	—	—	3.6	FMS	E	2
671230	04:19:00.	44.63	12.01	33.00	49	11	140	3	248	79	—	—	—	5.2	FMS	C	1
680622	12:21:37.	45.80	11.21	24.00	306	32	61	32	184	40	—	—	—	4.5	FMS	E	2
680622	12:37:51.	45.75	11.24	23.00	279	18	33	52	177	32	—	—	—	4.1	FMS	E	2
690106	22:03:00.	44.14	10.80	33.00	314	60	74	16	171	25	—	—	—	4.1	FMS	D	1
710715	01:33:00.	44.78	10.29	7.00	333	56	86	15	184	30	—	—	—	4.8	FMS	D	1
760506	19:59:06.	46.27	13.32	9.00	165	26	262	13	17	61	—	—	—	4.5	FMS	E	1
760506	20:00:11.	46.36	13.28	9.00	168	30	77	3	342	60	—	—	—	6.4	FMS	E	1
760507	00:23:50.	46.26	13.33	6.00	154	19	255	29	35	54	—	—	—	4.5	FMS	E	1
760508	03:10:06.	46.26	13.19	10.00	170	14	261	4	7	76	—	—	—	4.1	FMS	E	1
760509	00:53:45.	46.22	13.30	8.00	185	10	276	7	40	77	—	—	—	5.3	FMS	C	1
760510	04:35:52.	46.24	13.15	2.00	159	18	250	4	352	71	—	—	—	4.4	FMS	E	1
760511	22:44:01.	46.25	13.05	9.00	172	17	267	16	38	67	—	—	—	4.8	FMS	C	1
760608	12:14:38.	46.31	13.25	10.00	167	9	263	31	63	57	—	—	—	4.3	FMS	E	1
760626	11:13:47.	46.26	13.14	5.00	158	21	260	28	36	54	—	—	—	4.3	FMS	E	1
760714	05:39:34.	46.35	13.29	3.00	167	10	264	33	62	55	—	—	—	4.2	FMS	E	1
760911	16:31:12.	46.28	13.16	16.00	166	28	76	0	346	62	—	—	—	5.2	FMS	E	1
760911	16:35:02.	46.27	13.27	4.00	161	31	256	8	358	58	—	—	—	5.6	FMS	E	1
760912	19:53:28.	46.31	13.22	3.00	173	20	266	7	14	68	—	—	—	4.1	FMS	E	1
760913	18:54:46.	46.29	13.20	5.00	161	12	259	33	54	54	—	—	—	4.3	FMS	E	1
760915	03:15:19.	46.30	13.20	10.00	155	10	61	23	268	65	—	—	—	5.7	FMS	E	1
760915	04:38:54.	46.29	13.16	12.00	133	34	230	11	335	53	—	—	—	4.7	FMS	E	1
760915	09:21:19.	46.30	13.14	9.00	174	2	264	3	52	87	—	—	—	6.1	FMS	E	1
760915	09:45:57.	46.30	13.30	15.00	162	7	258	39	63	50	—	—	—	4.3	FMS	E	1
760915	19:31:11.	46.29	13.19	3.00	170	14	266	22	51	64	—	—	—	4.1	FMS	E	1
761213	05:24:03.	45.92	10.83	2.00	122	26	222	22	354	55	—	—	—	4.5	FMS	E	2
770403	03:18:14.	46.29	13.16	5.00	225	14	317	9	77	73	—	—	—	4.5	FMS	E	1
770716	13:13:31.	46.32	14.36	3.00	78	27	348	0	257	63	—	—	—	4.3	FMS	C	1
770916	23:48:08.	46.25	13.00	11.00	178	25	269	2	4	65	—	—	—	5.1	FMA	B	1
780220	12:13:34.	46.45	13.27	7.00	15	44	275	10	175	44	—	—	—	4	FMS	E	1
780403	10:49:46.	46.29	13.18	7.00	216	8	309	22	107	66	—	—	—	4.2	FMS	E	1
780512	15:39:00.	44.41	11.99	18.00	317	60	120	29	214	8	—	—	—	4.6	FMS	C	1
781212	15:14:49.	46.33	12.71	8.00	167	21	259	5	2	69	—	—	—	4.4	FMS	C	1
790306	13:46:06.	46.41	13.03	6.00	33	6	302	11	151	77	—	—	—	3.3	FMS	D	1
790418	15:19:20.	46.34	13.31	9.00	11	2	103	44	280	46	—	—	—	4.8	FMS	E	1
790619	10:03:15.	46.28	13.21	11.00	33	49	250	35	146	19	—	—	—	3.4	FMS	E	1
790814	18:58:58.	46.32	13.04	5.00	133	23	19	48	238	36	—	—	—	3.5	FMS	D	1
801014	13:33:27.	46.01	12.14	10.00	146	13	355	75	237	7	—	—	—	4	FMS	C	1
810628	06:16:27.	45.68	14.15	11.00	7	1	232	89	97	1	—	—	—	3.5	FMS	C	1
830617	16:36:09.	46.33	12.86	2.1.00	172	15	274	37	63	49	—	—	—	0	FMS	D	1

Table A1 - continued.

date	time	lat.	long.	depth km	σ1 az	σ1 pl	σ2 az	σ2 pl	σ3 az	σ3 pl	A1 MPa	A2 MPa	A3 MPa	M	type	Q	ref
831109	16:29:51.	44.68	10.28	38.00	353	17	257	19	123	64	—	—	—	4.9	FMS	B	1
831220	08:26:47.	46.31	13.21	11.00	3	2	272	30	97	60	—	—	—	0	FMS	C	1
830805	15:50:50.	45.96	14.08	1.00	42	26	275	50	147	26	—	—	—	3.7	FMS	E	1
841025	13:58:53.	45.64	14.34	11.00	206	45	302	6	38	44	—	—	—	3.5	FMS	E	1
860205	22:52:50.	46.27	12.72	7.00	217	7	314	43	120	46	—	—	—	0	FMS	C	1
860209	17:51:38.	46.38	13.03	7.00	343	10	80	33	238	55	—	—	—	0	FMS	C	1
860227	11:10:56.	46.51	11.57	17.00	19	35	209	55	111	0	—	—	—	3.1	FMS	C	2
860415	18:20:40.	45.77	10.74	8.00	102	4	209	70	13	16	—	—	—	3.2	FMS	C	2
860610	05:02:54.	46.33	12.51	8.00	148	1	283	89	58	1	—	—	—	2.9	FMS	D	1
860829	14:57:03.	46.38	12.46	6.00	317	14	133	76	227	1	—	—	—	4.4	FMS	C	1
860829	15:00:50.	46.37	12.46	3.00	114	7	20	32	215	57	—	—	—	3.8	FMS	E	1
910611	08:05:52.	46.22	12.94	2.20	139	5	231	24	37	65	—	—	—	3.9	FMS	D	1
920221	20:50:32.	45.46	14.33	11.00	231	13	325	18	107	68	—	—	—	4.1	FMS	D	1
—	—	46.63	13.68	0.236	302	22	39	16	162	63	35	18	9	—	OC	D	1
—	—	46.63	13.65	0.56	158	35	255	10	359	53	46	41	27	—	OC	C	1
—	—	46.93	14.57	0.12	108	18	206	24	346	60	27	13	9	—	OC	D	1
—	—	46.06	10.35	0.24	333	26	237	12	125	61	17.	13.	3.1	—	OC	D	1
—	—	46.18	10.35	0.25	328	13	130	76	233	3	37.	18.	14	—	OC	D	1
—	—	46.44	12.42	0.12	252	20	125	59	350	23	8.4	6.2	4.2	—	OC	D	1
—	—	46.55	12.62	0.28	10	60	210	28	116	8	8.6	7	3.7	—	OC	D	1

Corresponding author: Giuliana Rossi
Istituto Nazionale di Oceanografia e di Geofisica Sperimentale - OGS
Dipartimento di Geofisica della Litosfera; Borgo Grotta Gigante 42/c, Sgonico (Trieste), Italy
phone: +39 0402140347; fax: +39 040327307; e-mail: grossi@ogs.trieste.it